Desalination and Water Treatment
www.deswater.com
doi: 10.5004/dwt.2021.27816

239 (2021) 241–258
November

Investigation on the adsorption characteristics of Pb(II) onto bone char

Jinli Zhang[a], Gang Li[b,*], Jia Liu[c]

[a]*State Key Laboratory of Coastal and Offshore Engineering, Dalian University of Technology, Dalian, Liaoning 116024, China, Tel. +86-13940949667; email: jlzhang@dlut.edu.cn*
[b]*Shaanxi Key Laboratory of Safety and Durability of Concrete Structures, Xijing University, Xi'an, Shaanxi 710123, China, Tel. +86-15991735077; email: T_bag945@126.com*
[c]*School of Geological Engineering and Geomatics, Chang'an University, Xi'an, Shaanxi 710054, China, Tel. +86-15929935077; email: 15929935077@163.com*

Received 21 April 2021; Accepted 14 September 2021

ABSTRACT

The adsorption characteristics of Pb(II) onto bone char were studied by conducting batch experiments, and the influence of the solid–liquid ratio, pH, ionic strength, reaction time, temperature, and initial concentration on Pb(II) adsorption was evaluated. Based on the adsorption kinetic and isothermal adsorption characteristics of Pb(II), Cd(II), Ni(II), and Cu(II), the competitive adsorption characteristics between heavy metal ions in the multi-component system were explored. The results reveal that bone char exhibits a relatively high adsorption capacity for Pb(II). The adsorption capacity reached 158.36 mg g^{-1} when the initial concentration was 200 mg L^{-1}, the solid–liquid ratio was 1.0 g L^{-1}, the temperature was 20°C, and the optimum pH was 2–3. Furthermore, Pb(II) adsorption onto bone char was substantially affected by the solid–liquid ratio and the pH, and less affected by the ionic strength. Langmuir model fit the isothermal processes better than the Freundlich model, and the coefficients of determination were larger than 0.970. Pseudo-second-order kinetic model was best fitted to the adsorption kinetic processes of Pb(II), Cd(II), Ni(II), and Cu(II), which had the coefficients of determination larger than 0.990. Moreover, Cd(II) and Ni(II) had a low impact on the adsorption capacity of bone char to Pb(II), while Cu(II) showed a significant impact.

Keywords: Bone char; Metals; Adsorption kinetic; Isothermal adsorption

1. Introduction

The wastewaters discharged by industrial enterprises contain varying concentrations of heavy metal ions. If the wastewater treatment process does not meet standards or if wastewater is directly discharged, heavy metal pollution can directly enter soil and water bodies via the wastewater. According to the recent survey on groundwater pollution by the Ministry of Water Resources of China, 60% of the groundwater in China is contaminated to varying degrees. The pollution caused by industrial production cannot be ignored. In China, water and soil pollution has had a severe impact on economic and social development. Heavy metals cannot be degraded and removed from soil and water but rather accumulate in animals or plants and then accumulate by the food chain, possibly damaging human organs and posing a severe threat to human health [1]. Common methods for removing heavy metals include chemical precipitation, membrane treatment, ion exchange, and adsorption [2]. The adsorption method has been extensively studied due to its cost-effectiveness, versatile feasibility and environmental friendliness, and its reliability in removing heavy metal ions has been successfully verified. Studies have indicated that heavy metal ions (Ni(II), Zn(II), Mn(II), Hg(II), Pb(II), As(III), As(V), Cd(II), Cr(VI), and Cu(II)) can be effectively removed from wastewater by Pliocene clays

* Corresponding author.

[3], sunflower biochar [4], bentonite nanocomposites [5], modified bamboo [6], modified kapok fiber [7], modified fir biochar [8], activated carbon/zirconium oxide composites [9], and modified carbon adsorbent [10].

Studies have shown that synthetic hydroxyapatite can be used as an adsorbent to effectively removes heavy metal ions. The main component of animal bones, corals, and eggshells is hydroxyapatite, and animal bones are an inexpensive material that can be recycled. The bone char after treatment possesses a large specific surface area, high porosity, and satisfactory stability and can be used as a new biosorbent to treat wastewater. Rojas-Mayorga et al. [11] noted that the adsorption capacity of bovine bone char ranged from 68.3 to 119.4 mg g^{-1}, and the removal effect of Cd(II) was better than that of Zn(II) and Ni(II). Begum et al. [12] concluded that the maximum adsorption capacity of As(V) onto bone char reached 0.13 mg g^{-1}, and the Langmuir model and second-order kinetics model accurately fit the test results. To investigate the adsorption characteristics of Cr(III) onto bone char, Flores-Cano et al. [13] pointed out that the adsorption capacity increased by 2.6 times as the pH changed from 3 to 5, whereas the adsorption capacity reduced by 1.3 times as the temperature increased from 25°C to 35°C. Maria and Mansur [14,15] investigated the adsorption characteristics of manganese onto bone char by mathematical models and found that the diffusion model could well describe the manganese adsorption for distinct particle sizes, whereas the shrinking core model was more accurate for larger adsorbent particles and the mass transfer phenomena within spherical adsorbent particles. Based on the combination of Fe_3O_4 particles and bone char, Soltani et al. [16] found that the adsorption ability of As(V) onto nanocomposites increased with increasing dose and initial concentration, whereas decreased with increasing temperature, and the maximum adsorption ability reached 112 ug g^{-1}. Hernandez-Hernandez et al. [17] studied the adsorption behaviors of Cu(II) and Zn(II) onto bone char and found that stratified adsorption columns were better than conventional bed columns, and the adsorption process was more evident for Zn(II) than Cu(II). Martins et al. [18] revealed that the adsorption ability of Cu(II) onto bone char reached 1.093 mmol g^{-1}, which was higher than that of Cd(II) and Ni(II), and the Langmuir model fit the test results better than the Freundlich model. Ranjbar et al. [19] studied the adsorption of Cr(VI) onto bone char-ZnO composites and concluded that the removal rate increased as the adsorbent dose, shaking rate, temperature, and contact time increased, suggesting that the composite is a potential adsorbent for wastewater treatment. Sellaoui et al. [20] revealed that the adsorption ability of bone char to Cu(II) was significantly higher than that of Cd(II) and Zn(II), and a statistical model considering thermodynamic equilibrium was established. Gordillo-Ruiz et al. [21] constructed a neural network model to investigate the adsorption characteristics of Cd(II), Ni(II), and Zn(II) onto bone char and found that the new model was superior to the traditional model. Park et al. [22] reported that chicken bone char could be used as an effective adsorbent for Pb(II) removal, and the maximum adsorption ability reached 263 mg g^{-1}. Wang et al. [23] investigated the adsorption behavior of Cu(II) onto bovine bone char and found that the adsorption ability varied from 72.53 to 83.71 g kg^{-1} and that rib bone char had a better adsorption ability. Based on modified bone char, Yang et al. [24] pointed out that the volatile organic compounds adsorbent was more effective in a hierarchical structure which containing abundant adsorption sites, and the adsorption characteristics could be well described by the pseudo-second-order model. Medellin-Castillo et al. [25] noted that bone char was effective in removing fluoride and Cd(II) from solutions, and the adsorption ability for fluoride increased with pH decreased, while the adsorption ability for Cd(II) increased with pH increased.

As an additive or main heavy metal material, lead is extensively used in electricity storage, leather, petrochemicals, dyestuff, and ceramics. Lead can accumulate in human blood, cause nervous system disorders, destroy kidney function and liver function, and affect brain development in children, leading to mental retardation in severe cases [26]. Previous studies have indicated that bone char has an excellent adsorption capacity for metal ions (Cd(II), Cu(II), Zn(II), Ni(II), As(V), Cr(III), and Cr(VI)). To date, relatively few studies have examined the adsorption characteristics of Pb(II) onto bone char, especially the competitive adsorption characteristics between Pb(II) and other heavy metal ions. In this paper, the adsorption characteristics of Pb(II) onto bone char were studied by conducting batch experiments. The effects of the solid–liquid ratio, pH, ionic strength, initial concentration, and temperature on the adsorption characteristics of Pb(II) were analyzed, and the competitive adsorption characteristics between Pb(II), Cd(II), Ni(II), and Cu(II) in the multi-component system were explored.

2. Materials and methods

2.1. Materials

A commercial bone char (Shijiazhuang Baoqian Trading Co., Ltd., China) was used. Following sample pulverization by a high-speed pulverizer, the particles were passed through a sieve (0.025 mm) to meet the requirements of the experiments. The pulverized bone char was placed in an oven at 60°C for 24 h and then cooled and stored in a desiccator for future use. X-ray fluorescence spectrometry analysis showed that the main chemical components of the bone char were CaO and P_2O_5, which accounted for 49.9% and 47.5% by mass, respectively, and their total percentage exceeded 97.0% (as shown in Table 1). Table 2 shows the physical properties of bone char based on Brunauer–Emmett–Teller (BET) analysis.

The concentration of the stock solution was 1,000 mg L^{-1}, which was produced by dissolving 1.598 g of analytically pure $Pb(NO_3)_2$ in 1 L of distilled water, and the Pb(II) solution used in the experiment was prepared by diluting the stock solution.

2.2. Characterization techniques

X-ray fluorescence spectrometry (SRS 3400, Bruker, Germany) was used to characterize the chemical components of the adsorbent. BET analysis (NOVA 2200e, Quantachrome, USA) was employed to determine the surface area, pore size and pore volume. Fourier-transform infrared (FTIR) spectrophotometry (Nicolet 6700, Thermo Fisher Scientific,

Table 1
Chemical composition of bone char

Chemical component	Mass percent (%)
CaO	49.9
P_2O_5	47.5
MgO	0.890
SiO_2	0.433
Al_2O_3	0.389
SO_3	0.359
Fe_2O_3	0.260
Cl	0.078
SrO	0.071
K_2O	0.056
ZnO	0.054
CuO	0.026
ZrO_2	0.017

Table 2
Physical properties of bone char

Bulk density (kg m^{-3})	640
Pore size (nm)	7.5–60
Pore volume (cm^3 g^{-1})	0.225
Surface area (m^2 g^{-1})	100.06

USA) was used to identify the functional groups on the surface of the adsorbent with spectra in the wavenumber range of 4,000–400 cm^{-1}. X-ray diffraction (XRD) (X'Pert Pro, PANalytical B.V., Holland) with a 2θ range of 0°–80° was used to examine the mineralogical characterization. Atomic absorption spectrophotometry (AA6000, Shanghai Tianmei Biochemical Engineering Equipment Co., Ltd., China) was used to measure the metal concentration of the supernatant. A pH meter [Starter 2C, Ohaus Instruments (Shanghai) Co., Ltd., USA] was used to measure the pH of the supernatant. In addition, an oven (DHG-9011A, Shanghai Jing Hong Laboratory Instrument Co., Ltd., China), a thermostatic oscillator (SHA-C, Guohua Electric Appliance Co., Ltd., China) and a centrifuge (CT15RT, Shanghai Tianmei Biochemical Engineering Equipment Co., Ltd., China) were used during the experiments.

2.3. Experimental methods

Erlenmeyer flasks containing the samples were numbered and placed in a constant temperature oscillator. The temperature of the shaker was adjusted to a predetermined value, and the shaker was operated at a constant temperature for 12 h at a speed of 120 r min^{-1}. The solution following the reaction was filtered through filter paper, and the supernatant was collected. An atomic absorption spectrophotometer was used to measure the concentration in the supernatant, and a pH meter was used to measure the pH of the supernatant before and after the reaction (pH_0 and pH_e, respectively).

The adsorption ability at equilibrium q_e (mg g^{-1}), the removal rate R (%), and the experimental solid–liquid ratio r (g L^{-1}) were calculated from the following equations:

$$q_e = \frac{\left(C_0 - C_e\right)}{m} \times V \tag{1}$$

$$R = \frac{\left(C_0 - C_e\right)}{C_0} \times 100\% \tag{2}$$

$$r = \frac{m}{V} \tag{3}$$

where C_0 and C_e are the initial and equilibrium concentrations (mg L^{-1}), respectively, V is the solution volume (L), and m is the mass of bone char (g).

2.4. Theoretical models

2.4.1. Isothermal adsorption models

- Langmuir model [27]

$$\frac{C_e}{q_e} = \frac{1}{bQ} + \frac{C_e}{Q} \tag{4}$$

where C_e is the equilibrium concentration (mg L^{-1}), q_e is the adsorption capacity at equilibrium (mg g^{-1}), Q is the single-layer maximum adsorption capacity (mg g^{-1}), and b is the model constant (L mg^{-1}).

$$R_L = \frac{1}{1 + bC_0} \tag{5}$$

where R_L is the separation factor (dimensionless), b is the Langmuir model constant (L mg^{-1}), and C_0 is the initial concentration (mg L^{-1}).

The R_L value indicates whether the adsorption reaction is favorable [28]. When $0 < R_L < 1$, the reaction is favorable for adsorption. When $R_L > 1$, it is unfavorable for adsorption. When $R_L = 1$, the adsorption is reversible. When $R_L = 0$, it is irreversible [29].

- Freundlich model [30]

$$\log q_e = \log K_F + \frac{1}{n} \log C_e \tag{6}$$

where q_e is the adsorption capacity at equilibrium (mg g^{-1}), C_e is the equilibrium concentration (mg L^{-1}), K_F is the model constant related to the adsorption capacity (mg g^{-1}), and n is the model constant related to the adsorption strength (dimensionless).

2.4.2. Adsorption kinetic models [31]

- Pseudo-first-order kinetic model

$$\frac{dq_t}{dt} = k_1\left(q_e - q_t\right) \tag{7}$$

Its integral form is as follows:

$$\log\left(q_e - q_t\right) = \log q_e - \frac{k_1}{2.303}t \tag{8}$$

where q_t and q_e are the adsorption capacity (mg g^{-1}) at time t and at equilibrium, respectively, and k_1 is the adsorption rate constant of the pseudo-first-order kinetics (min^{-1}).

- Pseudo-second-order kinetic model

The pseudo-second-order kinetic model can be expressed as:

$$\frac{dq_t}{dt} = k_2\left(q_e - q_t\right)^2 \tag{9}$$

Its integral is:

$$\frac{t}{q_t} = \frac{1}{k_2 q_e^2} + \frac{1}{q_e}t \tag{10}$$

where q_t and q_e are the adsorption capacity (mg g^{-1}) at time t and at equilibrium, respectively, and k_2 is the adsorption rate constant (g mg^{-1} min^{-1}).

When t approaches 0, h can be expressed as

$$h = k_2 q_e^2 \tag{11}$$

where k_2 is the adsorption rate constant (g mg^{-1} min^{-1}), q_e is the adsorption capacity at equilibrium (mg g^{-1}), and h is the initial adsorption rate (mg g^{-1} min^{-1}).

- Intraparticle diffusion model

$$q_t = k_{\text{int}} t^{1/2} + c \tag{12}$$

where q_t is the adsorption capacity (mg g^{-1}), k_{int} is the internal diffusion rate constant (mg g^{-1} min$^{-1/2}$), and c is the intercept, which is related to the thickness of the boundary layer (dimensionless).

2.4.3. Adsorption thermodynamic model [32]

The adsorption thermodynamic equation can be expressed as:

$$K_D = \frac{q_e}{C_e} \tag{13}$$

$$\ln K_D = \frac{\Delta S}{R} - \frac{\Delta H}{RT} \tag{14}$$

$$\Delta G = \Delta H - T\Delta S \tag{15}$$

where K_D is the distribution coefficient at the solid–liquid interface (mL g^{-1}), q_e is the adsorption capacity at equilibrium (mg g^{-1}), C_e is the equilibrium concentration (mg L^{-1}), R is the molar gas constant (8.314 J mol^{-1} K^{-1}), T is the thermodynamic temperature (K), ΔH is the enthalpy change (kJ mol^{-1}), ΔS is the entropy change (J mol^{-1} K^{-1}), and ΔG is the Gibbs free energy (kJ mol^{-1}).

3. Adsorption characteristics of Pb(II)

3.1. Effect of the solid–liquid ratio on Pb(II) adsorption

The V of Pb(II) was fixed to 50 mL in the experiment, and the r was adjusted by varying the bone char mass. The r exhibits a certain effect on the adsorption ability and the removal rate of Pb(II). The C_0 was 200 mg L^{-1}, the experimental temperature was 20°C, and the pH was not adjusted during the experiment. Then, r was increased from 0.2 to 2.0 g L^{-1} to analyze the impact on the adsorption and removal of Pb(II). As shown in Fig. 1, the R of Pb(II) by bone char increased correspondingly when r was varied from 0.2 to 2.0 g L^{-1}. The reason is that as r increases, the mass of bone char increases, as does the number of adsorption sites [33]. However, the amount of Pb(II) adsorbed by bone char decreased with increasing r. The reason for this phenomenon is that after the mass of the bone char increases, some of the bone char particles aggregate, resulting in incomplete mixing of the bone char particles with the Pb(II) solution and a failure to completely expose the adsorption sites of the bone char [34].

3.2. Effect of pH on Pb(II) adsorption

When the pH is less than 6, Pb(II) in solution exists in the form of Pb^{2+}; when the pH is more than 6, the concentration of Pb^{2+} in the solution decreases rapidly. In this experiment, it was concluded that when the initial pH exceeded 5.5, a small amount of precipitates started to appear. To prevent precipitation, the pH was controlled to less than 5.5 in the experiment. To study the effect of pH on Pb(II) adsorption, r was kept at 1 g L^{-1}, the C_0 was 200 mg L^{-1}, the temperature was 20°C, and the initial pH (pH_0) was controlled with HNO_3 and NaOH. The impact of pH on the adsorbed amount of Pb(II) and the pattern of change in the solution pH after the reaction (pH_e) was analyzed, and the results are shown in Fig. 2.

When the solution pH was less than 2, some of the bone char was dissolved by the acid, and the H^+ in the solution occupied a certain number of adsorption sites. As a result, the capacity of the bone char to adsorb Pb(II) was greatly reduced, and the amount of adsorbed Pb(II) was low [35]. As the pH increased to a suitable range (e.g., approximately 2.5), the decomposition of hydroxyapatite $Ca_{10}(PO_4)_6(OH)_2$ (CaHA)-the effective component in the bone char was promoted. Subsequently, the decomposition products reacted with Pb(II) in solution to form a precipitated mineral, pyromorphite $Pb_{10}(PO_4)_6(OH)_2$ (PbHA), and the highest amount of Pb(II) adsorbed by bone char was reached at this time [36]. When the pH exceeded 3.5, the adsorption amount decreased slightly, mainly due to the formation of a soluble hydroxyl complex. Our analysis indicates that a suitable acidic environment is beneficial to Pb(II) removal by bone char.

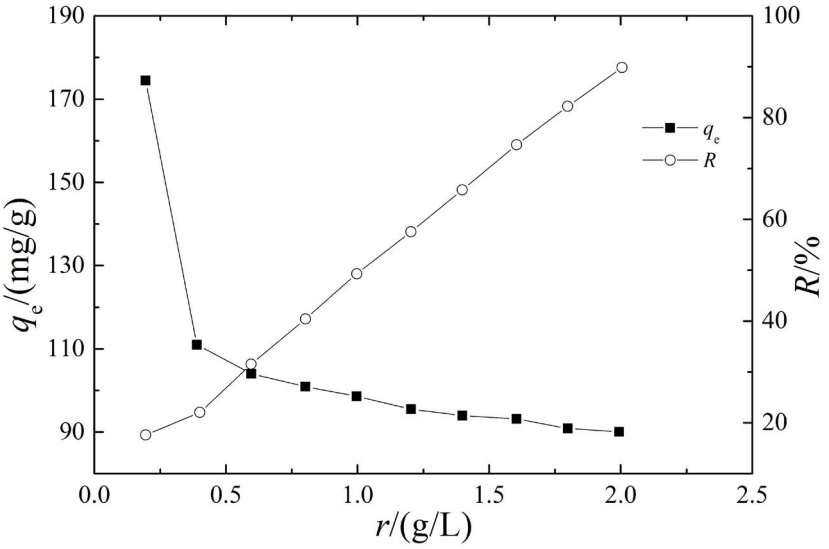

Fig. 1. Relationship between q_e or R and r for Pb(II) adsorption.

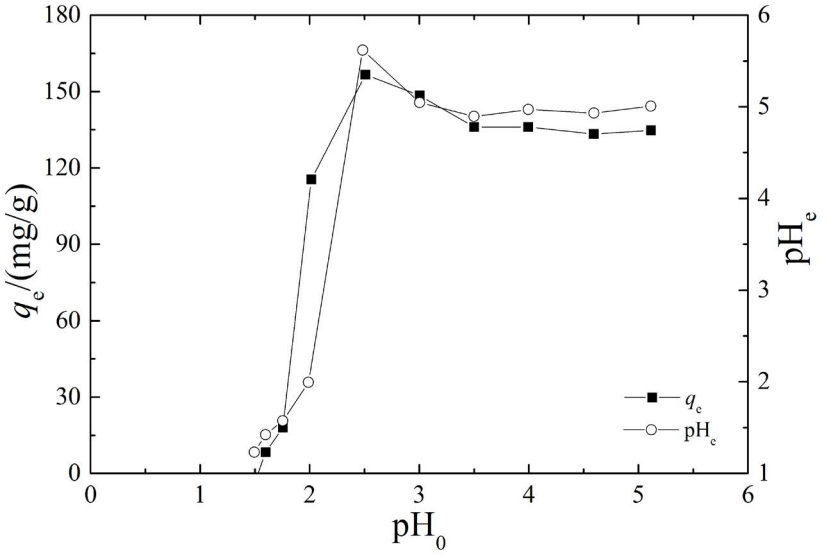

Fig. 2. Relationship between q_e or pH_e and pH_0 for Pb(II) adsorption.

$$\equiv P-O^- + H^+ \rightarrow \equiv P-OH \quad (16)$$

$$Ca_{10}(PO_4)_6(OH)_2 + 14H^+ \rightarrow 10Ca^{2+} + 6H_2PO_4^- + 2H_2O \quad (17)$$

$$10Pb^{2+} + 6H_2PO_4^- + 2H_2O \rightarrow Pb_{10}(PO_4)_6(OH)_2 + 14H^+ \quad (18)$$

3.3. Effect of ionic strength on Pb(II) removal

To investigate the effect of ionic strength on the removal of Pb(II), r was fixed at 1 g L^{-1}, the C_0 was 200 mg L^{-1}, and the temperature was set at 20°C. The ionic strength of the solution was controlled between 0.0025 and 0.5 mol L^{-1} by adding different concentrations of NaCl, and the R of Pb(II) under different ionic strengths was analyzed. As shown in Fig. 3, when the ionic strength in the solution was less than 0.05 mol L^{-1}, the R of Pb(II) by bone char decreased slightly, indicating that a certain competitive adsorption relationship exists between Na^+ and Pb^{2+}. When the ionic strength was equal to 0.05 mol L^{-1}, the electric double layer at the adsorption site was compressed [37], the thickness of the electric double layer was decreased, and the adsorption distance of Pb(II) in the solution on the bone char was reduced, thereby the R was increased. When the ionic strength of the solution changed from 0.05 to 0.5 mol L^{-1}, the effect of the competitive adsorption between Na^+ and Pb^{2+} was more prominent than that of the electric double layer, and the R showed a downward trend. The results revealed

that the overall ability of bone char to remove Pb(II) is less affected by the ionic strength [38].

3.4. Adsorption kinetics characteristics of Pb(II)

In this experiment, r was 1 g L^{-1}, the temperature was 20°C, the C_0 were 200, 300, and 500 mg L^{-1}, and the pH was not changed during the experiment. The relationship between the adsorbed amount and t was analyzed, and the results are shown in Fig. 4. The removal of Pb(II) by bone char was a fast reaction process; the amount of adsorbed Pb(II) exceeded 95% in the first 20 min, and the adsorption attained equilibrium within 30 min. In the initial stage, there were a large number of adsorption sites on the surface of the bone char, so Pb(II) was easily adsorbed, and the reaction rate was fast. With increasing t, the number of adsorption sites on the surface decreased, the concentration difference between the solid and liquid decreased, and the reaction rate between the adsorption sites inside the bone char particles and Pb(II) decreased. For the three different C_0, as the C_0 increased, and the adsorbed amount of Pb(II) increased correspondingly, but the adsorption reaction rate was essentially the same, which is consistent with previous research results [37].

Fig. 5 shows the fitted curve of the experimental results by the adsorption kinetic models. Table 3 lists the model parameters and R^2 values. Compared with pseudo-first-order and intraparticle diffusion models, the pseudo-second-order kinetic model provided an excellent fitting to the experimental results. The model assumes that the adsorption process is divided into two stages, fast adsorption and slow adsorption, which is consistent with the adsorption reaction process of bone char. Fig. 5c shows the fitted result of the intraparticle diffusion model, which contains an initial stage

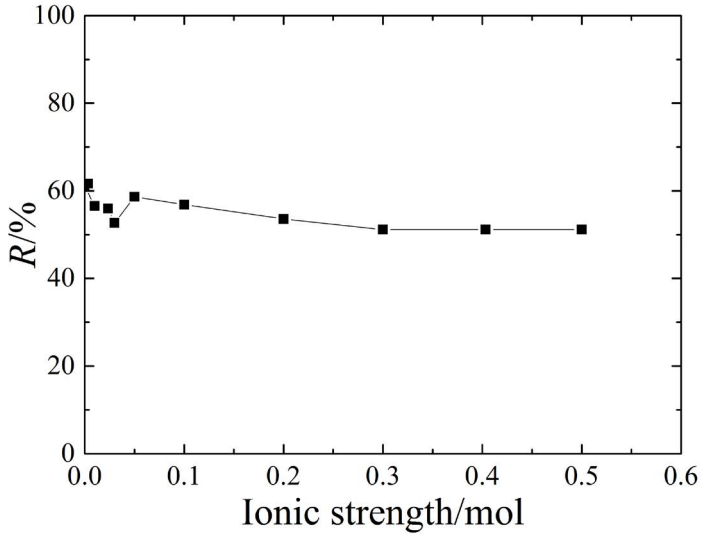

Fig. 3. Relationship between R and ionic strength for Pb(II) adsorption.

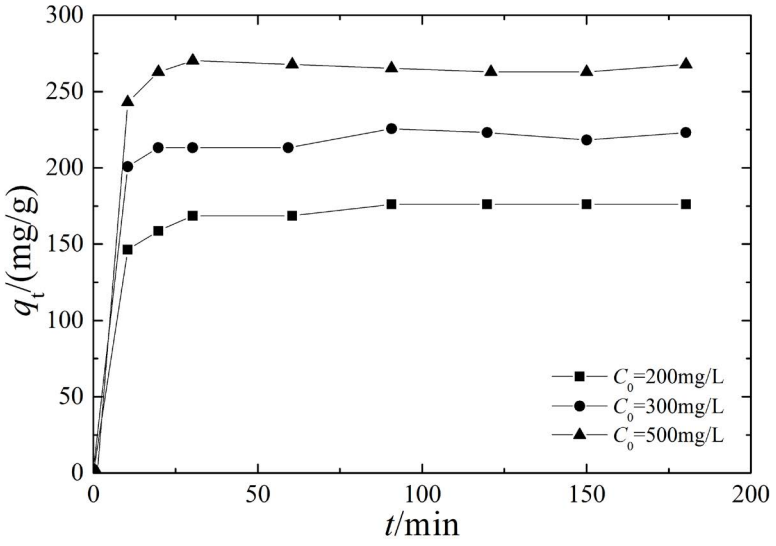

Fig. 4. Relationship between q_t and t for Pb(II) adsorption.

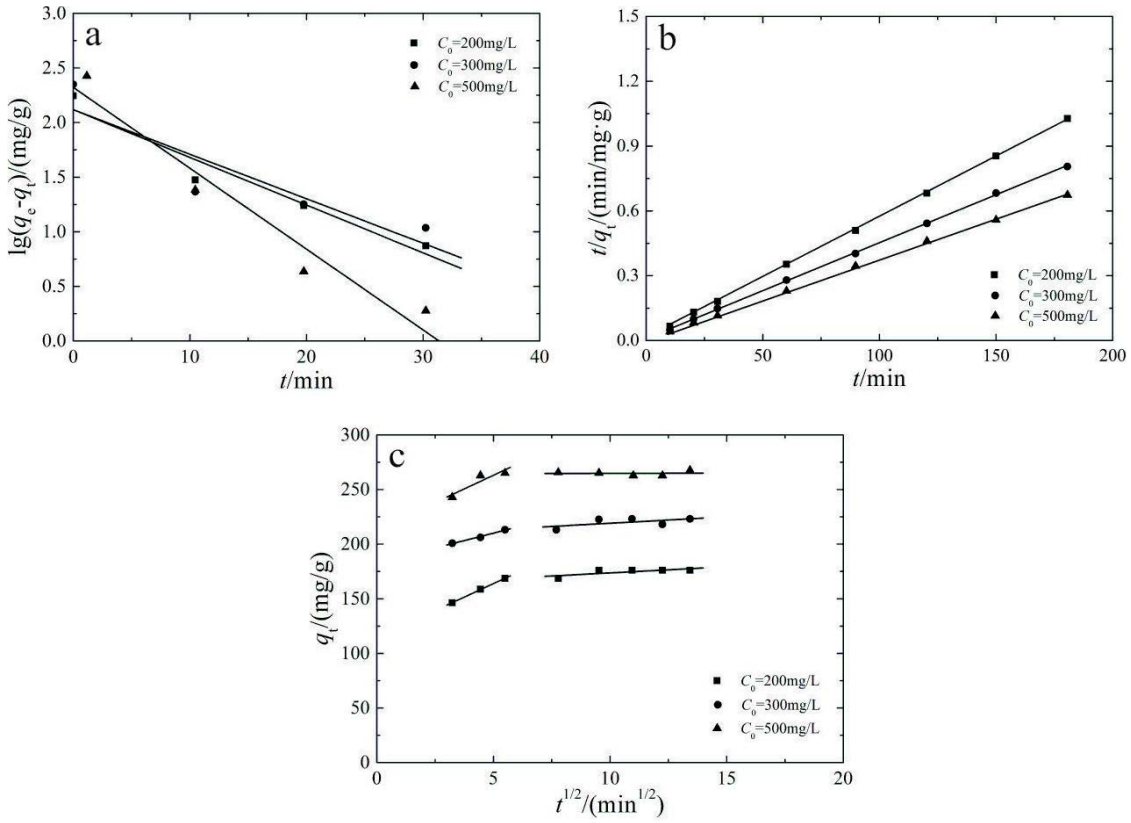

Fig. 5. Fitting curves of the adsorption kinetic models for Pb(II) adsorption (a) pseudo-first-order kinetic model, (b) pseudo-second-order kinetic model and (c) intraparticle diffusion model.

Table 3
Parameters of the adsorption kinetic models for Pb(II) adsorption

Model	Parameters	200 mg L^{-1}	300 mg L^{-1}	500 mg L^{-1}
Pseudo-first-order kinetic model	$q_{e,exp}$ (mg g^{-1})	174.79	224.08	267.14
	$q_{e,cal}$ (mg g^{-1})	131.24	131.14	209.83
	k_1 (min^{-1})	0.101	0.094	0.171
	R^2	0.9714	0.9042	0.9719
Pseudo-second-order kinetic model	$q_{e,cal}$ (mg g^{-1})	177.94	224.22	265.96
	k_2 (10^{-3} g mg^{-1} min^{-1})	2.589	2.677	10.027
	R^2	0.9998	0.9995	0.9997
Intraparticle diffusion model	k_{i1} (mg g^{-1} min$^{-1/2}$)	9.868	5.451	10.004
	c_1	114.500	182.809	213.064
	R_1^2	0.9997	0.9934	0.9275
	k_{i2} (mg g^{-1} min$^{-1/2}$)	1.131	1.173	0.049
	c_2	162.351	207.433	264.361
	R_2^2	0.7560	0.6060	0.0516

followed by linear and plateau stages. The initial stage was due to boundary layer sorption, the linear portion was due to intraparticle diffusion, and the plateau stage was due to equilibrium. This kind of intraparticle diffusion curve was also observed in other studies [39,40]. In addition, the boundary layer thickness (c) increased with increasing Pb(II) initial concentration, and c_1 was smaller than c_2, whereas k_{i1} was significantly larger than k_{i2}.

3.5. Isothermal adsorption characteristics of Pb(II)

In this experiment, r was 0.4 g L^{-1}, t was 12 h, the temperatures were 20°C, 30°C, 40°C, and 50°C, and various C_0 were used to analyze the characteristics of the isothermal adsorption of Pb(II). The experimental results are shown in Fig. 6. Under equilibrium adsorption conditions, the q_e of Pb(II) significantly increased with increasing C_e. The reason is that a

high C_0 can accelerate the decomposition of phosphate and produce adsorption sites [38], thereby improving the capacity of bone char to adsorb Pb(II). The adsorbed amount of Pb(II) increased slightly with increasing temperature, which indicated that the adsorption reaction is an endothermic process and that an increase in temperature favors the reaction.

The Langmuir and Freundlich models were used to describe the isothermal adsorption process of Pb(II). At different temperatures, the experimental results of Pb(II) adsorption onto bone char were fitted by the Langmuir and Freundlich adsorption models. The results are shown in Fig. 7, and Table 4 lists the corresponding model parameters. Both models provide an excellent fitting for the experimental results. The calculated R_L value is between 0 and 1, indicating that the adsorption of Pb(II) onto bone char is favorable. The Freundlich model parameter n is greater than 1, and the curve fitted by the Freundlich model is a type-I curve (a convex-upward shape), indicating that there is an affinity promoting the adsorption between the surface of the adsorbent and the adsorbate. K_F increased slightly as the temperature increased, suggesting that high temperatures are beneficial to the adsorption of Pb(II) onto bone char.

3.6. Adsorption thermodynamic characteristics of Pb(II)

To study the adsorption thermodynamics of bone char, linear fitting was performed, and the results are shown in Fig. 8. Based on the slope and intercept of the fitted line, the changes in the enthalpy ΔH, entropy ΔS, and Gibbs free energy ΔG during adsorption were obtained.

Because the C_0 of a solution has a large impact on the thermodynamic parameters, thermodynamic data fitting

Table 4
Parameters of the Langmuir and Freundlich models for Pb(II) adsorption

Model	Parameters	20°C	30°C	40°C	50°C
Langmuir model	Q (mg g^{-1})	492.611	495.050	518.135	526.316
	b (L mg^{-1})	0.034	0.039	0.044	0.050
	R^2	0.9790	0.9714	0.9781	0.9814
Freundlich model	K_F (mg g^{-1})	115.337	139.894	147.069	159.397
	n	4.022	4.670	4.597	4.825
	R^2	0.9805	0.9552	0.9703	0.9743

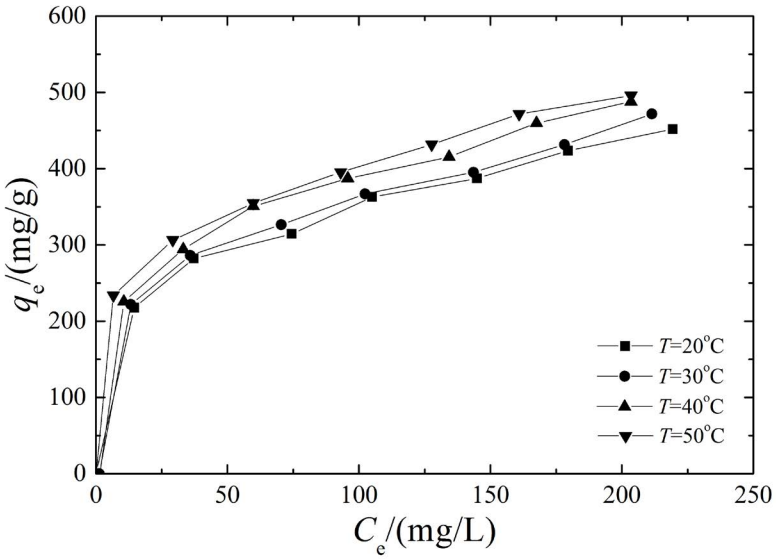

Fig. 6. Relationship between q_e and C_e for Pb(II) adsorption.

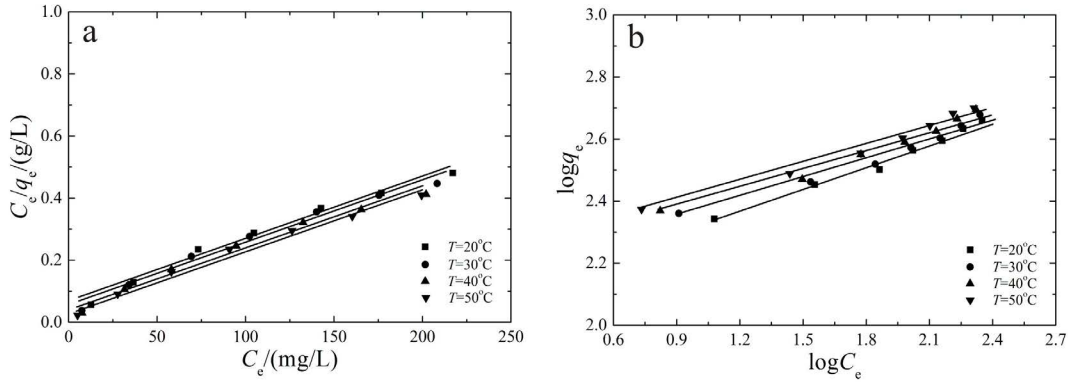

Fig. 7. Fitting curves of the isotherm models for Pb(II) adsorption (a) Langmuir model and (b) Freundlich model.

and parameter determination were performed at different C_0 in the experiment, and the results are shown in Table 5. When the C_0 of Pb(II) was changed from 100 to 110, 120, 130, 150, and 200 mg L^{-1}, the corresponding adsorption enthalpy change ΔH was 49.070, 22.600, 16.401, 15.650, 12.807, and 10.548 kJ mol^{-1}, respectively, and the corresponding adsorption entropy change ΔS was 185.96, 90.43, 66.05, 61.04, 48.12, and 35.93 J mol^{-1} K^{-1}, indicating that the changes in enthalpy and entropy during adsorption decrease with increasing initial Pb(II) concentration. Generally, positive ΔH denote that the adsorption is endothermic, whereas negative ΔH indicates an exothermic reaction. Therefore, the enthalpy change ΔH during adsorption always maintained a positive value, indicating that the adsorption process is an endothermic reaction. In addition, adsorption can be divided into physisorption and chemisorption based on the magnitude of the change in enthalpy. Physisorption ($2.1 < \Delta H < 20.9$ kJ mol^{-1}) is characterized by reversibility and weak bonding, and chemisorption ($80 < \Delta H < 200$ kJ mol^{-1}) is characterized by strong electrostatic forces that establish chemical bonds between the adsorbate and adsorbent. Table 5 shows that the ΔH ranged from 10.55 to 49.07 kJ mol^{-1}, indicating that it mainly physical and physicochemical adsorption [41,42]. The free energy change ΔG showed a negative value, indicating that the adsorption process was spontaneous. The C_0 of Pb(II) was fixed, and the change in Gibbs free energy ΔG decreased with increasing temperature, suggesting that an increase in temperature can promote the adsorption of Pb(II) and produce a better adsorption effect.

3.7. Comparison of the adsorption capacity

To analyze the adsorption characteristics of bone char and other adsorbents, Pb(II) was used as a target ion to measure the adsorption capacity under different experimental conditions. Table 6 shows the maximum adsorption capacities of Pb(II) for the adsorbents. The adsorption capacity of bone char reached 492.61 and 526.32 mg g^{-1} at 20°C and 50°C, respectively. Furthermore, the adsorption capacity of bone char was significantly higher than that of modified biochar, raw tamarind seeds, cacao activated carbon, apple tree branch biochar, white pottery clay, and modified bentonite and nearly similar to that of modified pomelo peels,

Table 5
Parameters of the thermodynamic model for Pb(II) adsorption

C_0 (mg L^{-1})	T (K)	ΔG (kJ mol^{-1})	ΔH (kJ mol^{-1})	ΔS (J mol^{-1} K^{-1})	R^2
100	293	–5.42	49.070	185.96	0.980
	303	–7.28			
	313	–9.14			
	323	–11.0			
110	293	–3.90	22.600	90.43	0.979
	303	–4.80			
	313	–5.71			
	323	–6.61			
120	293	–2.95	16.401	66.05	0.998
	303	–3.61			
	313	–4.27			
	323	–4.93			
130	293	–2.23	15.650	61.04	0.994
	303	–2.85			
	313	–3.46			
	323	–4.07			
150	293	–1.29	12.807	48.12	0.998
	303	–1.77			
	313	–2.26			
	323	–2.74			
200	293	–0.02	10.548	35.93	0.993
	303	–0.34			
	313	–0.70			
	323	–1.06			

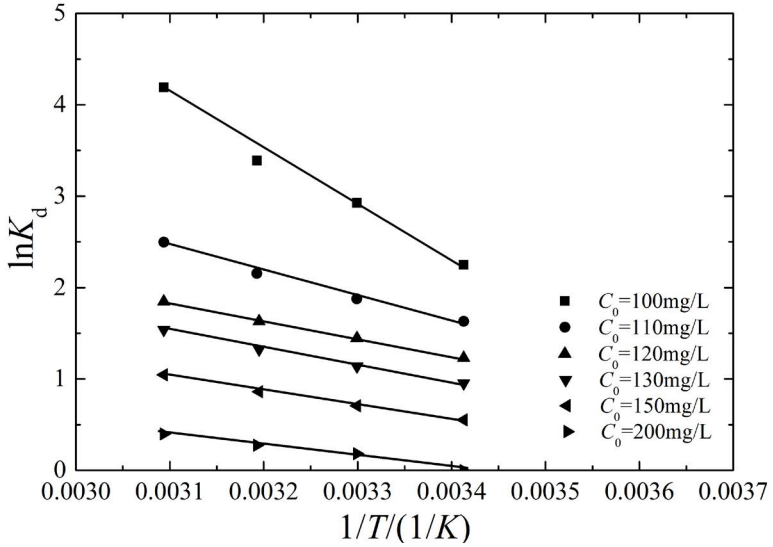

Fig. 8. Fitting curves of the thermodynamic model for Pb(II) adsorption.

Table 6
Comparison of maximum adsorption capacities of Pb(II) using various adsorbents

Adsorbent	pH	T (°C)	r (g L^{-1})	C_0 (mg L^{-1})	q_m (mg g^{-1})	References
KOH-modified N-enriched biochar	5.0	25	0.2	1,000	143.00	[43]
Modified pomelo peels	4.0	25	1.0	100–800	482.42	[44]
Raw tamarind seeds	6.0	30	3.5	25–150	16.00	[45]
Modified ginkgo leaves	5.0	–	0.5	50–350	551.60	[46]
Theobroma cacao activated carbon	6.4	30	4.0	25–150	47.17	[47]
Leonardite-derived humic acid	5.0	25	0.7	0–200	185.90	[48]
Hydroxyapatite from chicken eggshell	6.0	–	1.0	200–500	505.05	[49]
Cotton straw-derived biochar	5.5	25	5.0	5–300	124.70	[50]
Pure zeolite	5.0	–	0.3	10–200	432.57	[51]
Zeolite-carbon composite	5.0	–	0.3	10–200	321.91	[52]
Apple tree branch biochar	5–5.5	25	2.0	50–500	53.90	[53]
Maize stalk biochar	5–5.5	25	2.0	50–500	62.86	[53]
White pottery clay	5.5	20	1.0	80–280	155.04	[54]
Acid-modified bentonite	5.5	20	2.0	5–50	10.55	[55]
Rice husk biochar	5.0	40	2.0	5–50	37.20	[56]
Modify watermelon rind biochar	6.0	–	2.0	200	102.81	[57]
Manure biochar	–	23	1.5	300	50.41	[58]
Ti(IV) iodovanadate cation exchanger	6.0	20	2.0	10–60	18.80	[59]
Bone char	5.0	20	0.4	100–400	492.61	This study
Bone char	5.0	50	0.4	100–400	526.32	This study

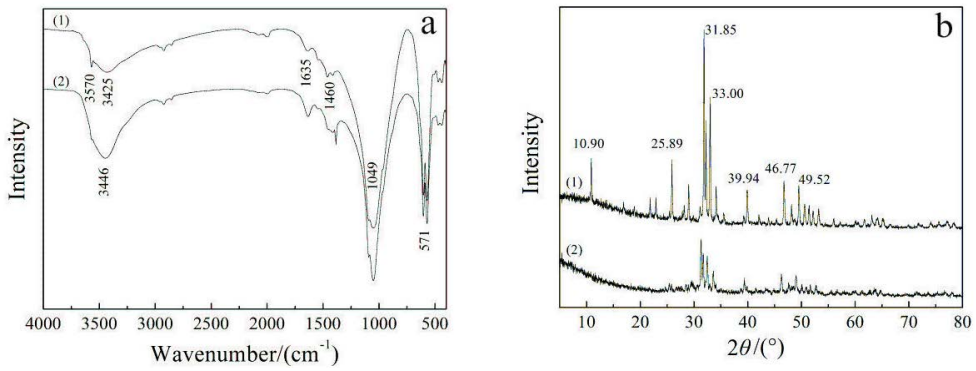

Fig. 9. FTIR and XRD spectra of bone char for Pb(II) adsorption with (1) unloaded and (2) loaded: (a) FTIR and (b) XRD).

modified ginkgo leaves, and hydroxyapatite from chicken eggshells. Therefore, it can be concluded that bone char shows an excellent adsorption capacity for Pb(II) and has extensive potential in wastewater treatment.

3.8. Adsorption mechanism of Pb(II)

To investigate the adsorption mechanism of Pb(II), the bone char-loaded Pb(II) before and after adsorption were analyzed by FTIR and XRD, and the results are shown in Fig. 9. A characteristic peak consistent with that of hydroxyapatite was found in the frequency range of 3,425 to 3,570 cm^{-1} in the infrared spectrum of bone char [60]; this peak corresponds to the stretching vibrations of –OH. In the infrared spectrum of Pb(II)-loaded bone char, the characteristic peak intensity in the frequency range of 3,425–3,570 cm^{-1} increased, mainly because the –OH anion in Ca–OH exchanged with other anions in solution and the content of free –OH increased [60]. This is also the reason for the increase in solution pH (i.e., pH_e) after the adsorption reaction.

Fig. 9b shows that the XRD diffraction pattern of bone char was similar to that of Pb(II)-loaded bone char, and no new diffraction peak was formed, suggesting that the secondary crystalline phase did not appear after the bone char was loaded with Pb(II).

When pH < pH_{pzc} (zero charge point), P–OH is the dominant surface functional group of bone char. When the pH is less than and close to pH_{pzc}, P–O– is dominant; when pH > pH_{pzc}, Ca–OH is dominant [61]. In the experiment, $\Delta pH = pH_e - pH_0 > 0$, that is, pH < pH_{pzc}. Therefore, the surface complexation can be expressed as [62].

$$P-OH+Pb^{2+}\rightarrow P-O-Pb^{2+}+H^{+} \quad (19)$$

When the pH is low and Pb^{2+} is present, the decomposition of CaHA can be promoted to release Ca^{2+} [63], and precipitates can be formed after the replacement of Ca^{2+} with Pb^{2+}. The above process can be described as:

$$Ca_{10}(PO_4)_6(OH)_2+xPb^{2+}\rightarrow Pb_xCa_{(10-x)}(PO_4)_6(OH)_2+xCa^{2+} \quad (20)$$

$$Ca_{10}(PO_4)_6(OH)_2+14H^{+}\rightarrow 10Ca^{2+}+6H_2PO_4^{-}+2H_2O \quad (21)$$

Fig. 10 shows the relationship between the Pb^{2+} and Ca^{2+} concentrations in the solution at equilibrium, thereby demonstrating the reaction process. In summary, the adsorption mechanism of Pb(II) onto bone char mainly includes surface complexation and CaHA decomposition-replacement-precipitation. These two processes are fast reactions, and adsorption equilibrium can be reached within 60 min.

4. Adsorption characteristics of multi heavy metal ions

4.1. Adsorption kinetic characteristics of Pb(II), Cd(II), Ni(II), and Cu(II)

In this experiment, r was 1 g L^{-1}, the temperature was 20°C, the C_0 was 100 mg L^{-1}, and the pH was not changed. The relationship between the adsorbed amounts of Pb(II), Cd(II), Ni(II), and Cu(II) and t were analyzed, and the results are shown in Fig. 11.

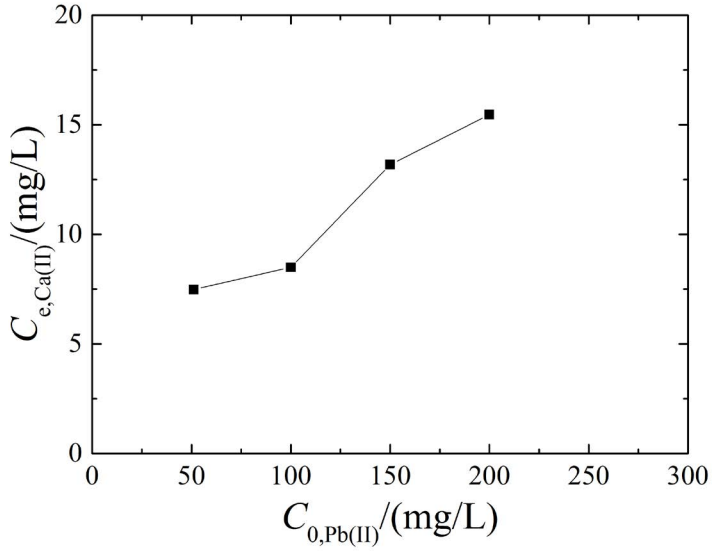

Fig. 10. Relationship between $C_{e,Ca(II)}$ and $C_{0,Pb(II)}$.

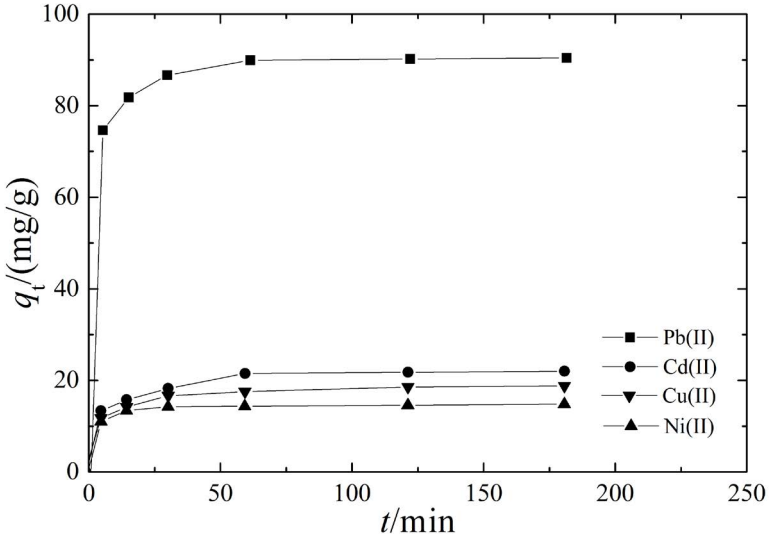

Fig. 11. Relationship between q_t and t for Pb(II), Cd(II), Cu(II), and Ni(II) adsorption.

The adsorption processes of Pb(II), Cd(II), Ni(II), and Cu(II) onto bone char were fast reactions: the amount of adsorbed heavy metals reached more than 90% in the first 30 min, and adsorption equilibrium was attained within 60 min. In the initial stage, a large number of adsorption sites existed on the surface of the bone char, the heavy metal ions could be easily adsorbed, and the reaction rate was fast. With increasing t, the number of surface adsorption sites decreased, the concentration difference between the solid and liquid decreased, and the reaction rate decreased between the adsorption sites inside the bone char particles and heavy metal ions.

The experimental results were fitted using the adsorption kinetic models, and the results are shown in Fig. 12. Table 7 lists the kinetic model parameters. Compared with pseudo-first-order and intraparticle diffusion models, the experimental amount of adsorbed heavy metals $q_{e,\exp}$ was very close to the theoretical adsorbed amount of heavy metals $q_{e,\mathrm{cal}}$, and the R^2 was as high as 0.999, indicating that the pseudo-second-order kinetic equation provided a satisfactory fit to the experimental results. The model assumes that the adsorption process involves fast adsorption and slow adsorption, which is consistent with the process of adsorption by bone char. Therefore, it is suitable to use the pseudo-second-order kinetic model to analyze the adsorptions of Pb(II), Cd(II), Ni(II), and Cu(II).

4.2. Isothermal adsorption characteristics of Pb(II), Cd(II), Ni(II), and Cu(II)

Fig. 13 reflects the relationship between the amount of adsorbed heavy metals at a certain temperature and the equilibrium concentration of the solution. In the experiment, r was 1 g L^{-1}, t was 12 h, and the temperature was controlled at 20°C. The isothermal adsorption characteristics of Pb(II), Cd(II), Ni(II), and Cu(II) onto bone char were analyzed.

The Langmuir and Freundlich models were used to describe the isothermal adsorption processes of Pb(II), Cd(II), Ni(II), and Cu(II). Table 8 shows the model parameters of two models. The adsorption capabilities of bone char for heavy metal ions in the Langmuir model were ordered as Pb(II) >> Cd(II) > Cu(II) > Ni(II). In the Freundlich model, the n of the bone char for Pb(II), Cd(II), Ni(II), and Cu(II) were all greater than 1, and the curve fitted by the Freundlich model was a type I curve (i.e., a convex-upward shape), indicating the presence of affinity promoting adsorption between the surface of the adsorbent and the adsorbate. The n values of all heavy metals were ordered as $n_{\mathrm{Pb(II)}} >> n_{\mathrm{Cu(II)}}$,

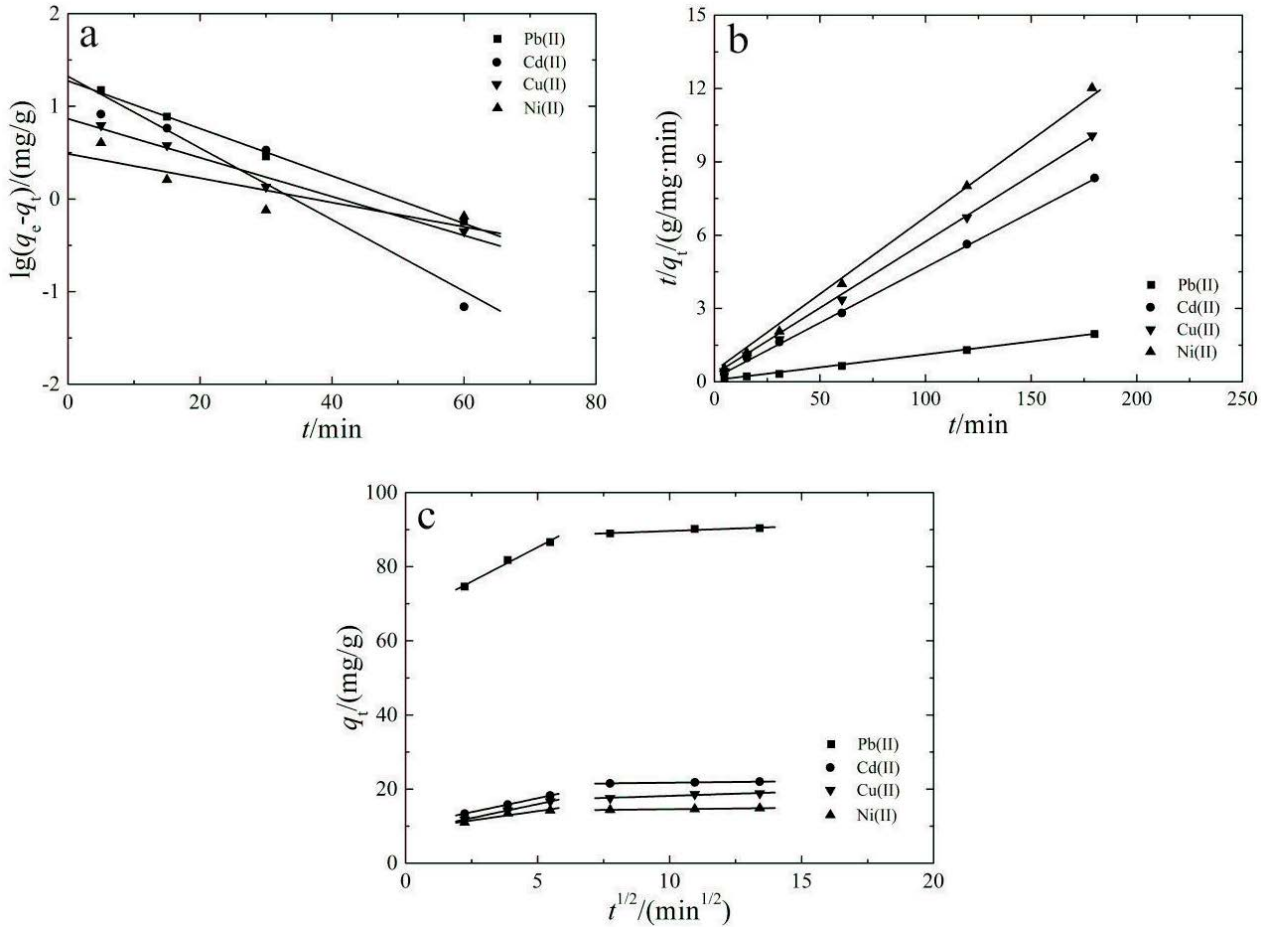

Fig. 12. Fitting curves of the adsorption kinetic models for Pb(II), Cd(II), Cu(II), and Ni(II) adsorption (a) pseudo-first-order kinetic model, (b) pseudo-second-order kinetic model and (c) intraparticle diffusion model.

Table 7
Parameters of the adsorption kinetic models for Pb(II), Cd(II), Ni(II), and Cu(II) adsorption

Model	Parameters	Pb(II)	Cd(II)	Ni(II)	Cu(II)
Pseudo-first-order kinetic model	$q_{e,exp}$ (mg g^{-1})	89.52	21.60	15.02	18.00
	$q_{e,cal}$ (mg g^{-1})	18.78	21.06	3.07	7.33
	k_1 (min^{-1})	0.059	0.089	0.030	0.048
	R^2	0.9985	0.9622	0.8663	0.9904
Pseudo-second-order kinetic model	$q_{e,cal}$ (mg g^{-1})	90.17	22.33	15.13	18.20
	k_2 (10^{-3} g mg^{-1} min^{-1})	0.011	0.009	0.063	0.031
	R^2	0.9998	0.9997	0.9994	0.9998
Intraparticle diffusion model	k_{i1} (mg g^{-1} min$^{-1/2}$)	3.712	1.502	1.013	1.502
	c_1	66.692	9.999	8.971	8.408
	R_1^2	0.9942	0.9999	0.9655	0.9999
	k_{i2} (mg g^{-1} min$^{-1/2}$)	0.263	0.081	0.081	0.226
	c_2	87.029	20.899	13.740	15.893
	R_2^2	0.9543	0.9979	0.9979	0.9614

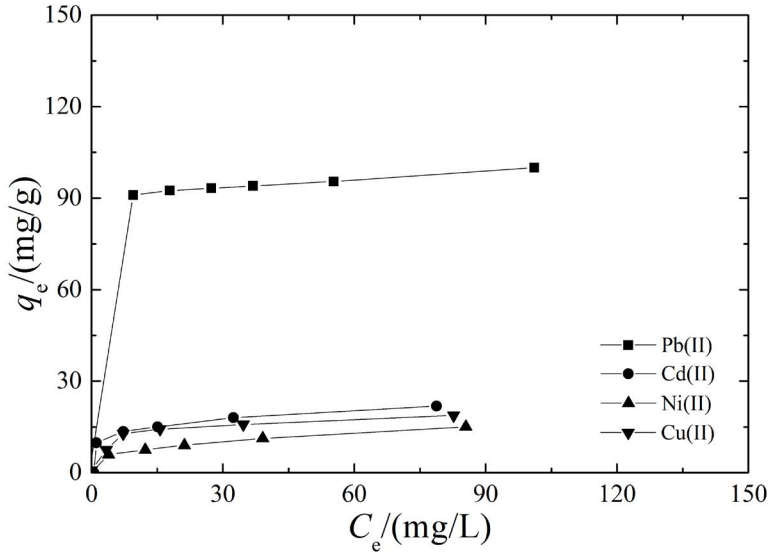

Fig. 13. Relationship between q_e and C_e for Pb(II), Cd(II), Ni(II) and Cu(II) adsorption.

Table 8
Parameters of the Langmuir and Freundlich models for Pb(II), Cd(II), Ni(II), and Cu(II) adsorption

Model	Parameters	Pb(II)	Cd(II)	Ni(II)	Cu(II)
Langmuir model	Q (mg g^{-1})	100.301	23.348	16.875	18.477
	b (L mg^{-1})	0.503	0.132	0.067	0.282
	R^2	0.999	0.995	0.949	0.994
Freundlich model	K_F (mg g^{-1})	82.966	5.923	3.936	9.103
	n	28.249	3.185	3.531	6.412
	R^2	0.863	0.920	0.944	0.996

$n_{Ni(II)}$, $n_{Cd(II)}$ > 1, and the corresponding K_F values were ordered as $K_{F,Pb(II)}$ >> $K_{F,Cu(II)}$, $K_{F,Cd(II)}$, $K_{F,Ni(II)}$, indicating that the capacity of bone char to adsorb Pb(II) and the affinity of bone char to Pb(II) are considerably larger than those of Cd(II), Ni(II), and Cu(II), which is consistent with the results of the Langmuir model.

Table 2 shows that the pore size of the bone char ranged from 7.5 to 60 nm, the pore volume attained 0.225 cm^3 g^{-1}, and the surface area reached 100.06 m^2 g^{-1}. The ionic radius of the hydrated heavy metal ion Pb(II) is smaller than that of the other three heavy metal ions (Pb(II) = 0.401 nm, Cd(II) = 0.426 nm, Cu(II) = 0.419 nm, and Ni(II) = 0.404 nm) [64,65]. Hydrated ions with a small ionic radius are more likely to be close to the mineral surface and to diffuse into the pores of the mineral [22,66–68], and the adsorption sites on the same surface area can adsorb a larger number of ions relative to hydrated ions with a larger ionic radius. The smaller the hydrated ionic radius is, the stronger the possibility that the metal ions can be adsorbed onto the mineral surface. The Pb(II) hydration energy is the smallest among the four heavy metal ions (Pb(II) = 1,481 kJ mol^{-1}, Cd(II) = 1,807 kJ mol^{-1}, Cu(II) = 2,100 kJ mol^{-1}, and

Ni(II) = 2,106 kJ mol^{-1}); therefore, a bare Pb(II) ion is more likely to be present and thus fixed by minerals. According to the model-fitting results, the Langmuir model is significantly better than the Freundlich model.

Through calculation, it was found that the separation factors obtained in the experiment all satisfied $0 < R_L < 1$, indicating that the adsorptions of Pb(II), Cd(II), Ni(II), and Cu(II) onto bone char were all favorable.

4.3. Competitive adsorption characteristics in the binary system

In actual engineering environments, the leachate may contain a variety of heavy metal ions, so it is necessary to consider the effect of other heavy metal ions on the adsorption of Pb(II) onto bone char. In this experiment, r was 1 g L^{-1}, t was 12 h, the temperature was controlled at 20°C, and the C_0 of Pb(II) varied from 100 to 200 mg L^{-1}. The influence of divalent ions on Pb(II) adsorption was analyzed by adding Cd(II), Ni(II), and Cu(II) at different C_0 in the range of 10 to 200 mg L^{-1}. The experimental results are shown in Fig. 14.

The Langmuir and Freundlich models were used to fit the experimental results, and the associated parameters are shown in Table 9. When the C_0 of Cd(II) and Ni(II) ranged from 0 to 200 mg L^{-1}, the Langmuir adsorption isotherm model provided a satisfactory fit for the adsorption of Pb(II) onto bone char; the R^2 was greater than 0.99. When different concentrations of Cu(II) were added to the system, the R^2 was greater than 0.988 if the C_0 of Cu(II) was not more than 50 mg L^{-1}; the R^2 was 0.147, 0.411, or 0.182 when the C_0 of Cu(II) was 50, 100, or 200 mg L^{-1}, respectively, indicating that the Langmuir isotherm adsorption model was no longer suitable. The Freundlich model provided an excellent fit for the effects of Cd(II) and Cu(II) on the adsorption of Pb(II) onto bone char; the R^2 ranged from 0.72 to 0.92. However, this model was not suitable for describing the effect of Ni(II) on Pb(II) adsorption, and the R^2 of the fitting result was small. The dimensionless factor satisfied $0 < R_L < 1$, indicating favorable adsorption.

In the competitive adsorption system of bimetal or multimetal ions, there is a finite number of total adsorption sites in the adsorbent, so the presence of other heavy metal ions in the adsorption system invariably produces an adverse effect on Pb(II) adsorption. The adsorption performance is determined mainly by the concentration of other ions and the selective adsorption of bone char. When the C_0 of Cd(II), Ni(II), and Cu(II) were less than 50 mg L^{-1}, the q_e of Pb(II) decreased as the C_0 of Cd(II), Ni(II) and Cu(II) increased, mainly because the heavy metal ions that were added externally occupied a certain number of adsorption sites on the surface of the bone char. When the C_0 of Cd(II), Ni(II), and Cu(II) exceeded 50 m g L^{-1}, the effect of increased C_0 on Pb(II) adsorption gradually stabilized. The divalent heavy metal ions Cd(II) and Ni(II) showed a low impact on Pb(II) adsorption. The main reason is that the adsorption affinity of bone char for Cd(II) and Ni(II) is smaller than that for Pb(II); thus, the Pb(II) in bone char is not easily desorbed

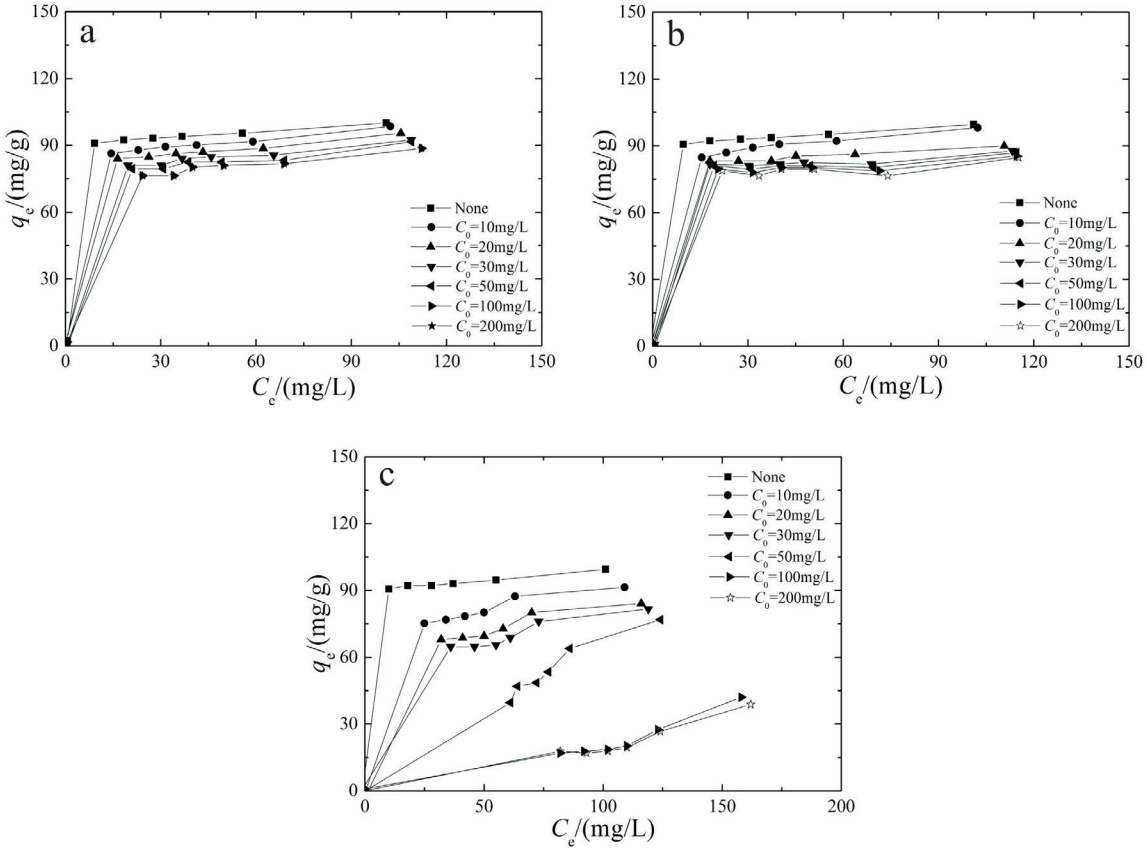

Fig. 14. Effect of Cd(II), Ni(II) and Cu(II) on Pb(II) adsorption (a) Cd(II), (b) Ni(II) and (c) Cu(II).

Table 9
Parameters of the Langmuir and Freundlich models in binary system

Model	Ion	Parameters	0 mg L^{-1}	10 mg L^{-1}	20 mg L^{-1}	30 mg L^{-1}	50 mg L^{-1}	100 mg L^{-1}	200 mg L^{-1}
Langmuir model	Cd(II)	Q (mg g^{-1})	100.301	100.301	97.182	94.340	93.633	92.593	92.166
		b (L mg^{-1})	0.503	0.258	0.233	0.202	0.169	0.152	0.149
		R^2	0.999	0.997	0.997	0.997	0.994	0.997	0.996
	Ni(II)	Q (mg g^{-1})	100.301	101.317	91.491	87.796	86.505	86.356	85.690
		b (L mg^{-1})	0.503	0.241	0.359	0.383	0.408	0.293	0.255
		R^2	0.999	0.999	0.999	0.997	0.998	0.996	0.992
	Cu(II)	Q (mg g^{-1})	100.301	99.404	94.429	95.057	–	–	–
		b (L mg^{-1})	0.503	0.103	0.067	0.048	–	–	–
		R^2	0.999	0.997	0.993	0.988	0.147	0.411	0.182
Freundlich model	Cd(II)	K_F (mg g^{-1})	82.966	71.846	69.178	64.288	61.817	55.971	55.951
		n	28.249	16.027	16.003	14.086	13.340	10.584	10.762
		R^2	0.863	0.862	0.823	0.834	0.725	0.911	0.866
	Ni(II)	K_F (mg g^{-1})	82.966	68.221	73.612	–	–	–	–
		n	28.249	12.979	25.278	–	–	–	–
		R^2	0.863	0.985	0.740	0.144	0.345	0.327	0.138
	Cu(II)	K_F (mg g^{-1})	82.966	47.075	35.955	28.736	1.202	0.027	0.044
		n	28.249	7.036	5.606	4.603	1.148	0.695	0.757
		R^2	0.863	0.907	0.874	0.859	0.918	0.886	0.850

Note: means R^2 is smaller and the model is unsuitable.

in the presence of Cd(II) and Ni(II), the exchange processes of Cd(II) and Ni(II) with Pb(II) adsorbed by bone char are restricted, and the amount of exchanged ions does not increase with increasing concentration. However, although the selective capacity of bone char to adsorb Pb(II) is considerably higher than that to adsorb Cu(II), the presence of Cu(II) significantly influences Pb(II) adsorption. When the C_0 of Cu(II) exceeded 50 mg L^{-1}, the ability of bone char to adsorb Pb(II) was substantially reduced.

4.4. Competitive adsorption characteristics in the quaternary system

To study the competitive adsorption characteristics in the quaternary system, r was 1 g L^{-1}, t was 12 h, the temperature was controlled at 20°C, and the pH was not changed during the experiment. The ratio of the C_0 of Pb(II), Cd(II), Ni(II), and Cu(II) was 1:1:1:1; that is, the C_0 of the mixed system solution in the table was 10 mg L^{-1}, indicating that the C_0 of Pb(II), Cd(II), Ni(II), and Cu(II) in the mixed solution were all 10 mg L^{-1}. The experimental results are shown in Table 10.

The q_e of Pb(II), Cd(II), Ni(II), and Cu(II) by bone char in the quaternary system were smaller than those in the mono component system because under a certain r, bone char has a finite number of total adsorption sites. In the multi component system, the adsorption sites are occupied by four heavy metal ions at the same time. Therefore, the amounts of all heavy metal ions adsorbed by bone char are lower than those in the mono component system. Note that although the C_0 were equal, the amounts of these metal ions adsorbed by the bone char in the quaternary system were different. The order of the adsorbed amount was consistent with that in the mono component system, and the q_e of Pb(II) by bone char was significantly higher, confirming again that bone char shows selective adsorption for Pb(II).

5. Conclusions

Bone char possesses a high selective adsorption capacity for Pb(II) and is a biosorbent with promising application prospects. Based on batch experiments, the adsorption characteristics of Pb(II) onto bone char were systematically studied, and the influence of the solid–liquid ratio, pH, ionic strength, and temperature on the adsorption characteristics was assessed. Additionally, the kinetic and thermodynamic adsorption characteristics of Pb(II) onto bone char were studied, and the corresponding adsorption mechanism was analyzed. In the binary system and quaternary system, the effects of other divalent heavy metal ions on the adsorption characteristics of Pb(II) onto bone char were evaluated. The main conclusions are as follows:

- Bone char possessed a high adsorption capacity for Pb(II). When the C_0 was 200 mg L^{-1}, r was 1.0 g L^{-1}, the temperature was 20°C, and the optimum pH was 2–3, the amount of adsorbed Pb(II) reached 158.36 mg g^{-1}. The r and pH substantially affected the Pb(II) adsorption onto bone char, whereas the ionic strength exhibited a low impact. Pb(II) adsorption onto bone char was a spontaneous and endothermic process. The adsorption mechanism of Pb(II) onto bone char mainly included surface complexation and CaHA decomposition-replacement-precipitation.
- The Langmuir model satisfactorily predicted the isothermal adsorption process of Pb(II), Cd(II), Ni(II), and Cu(II) onto bone char. Moreover, the pseudo-second-order kinetic model well described the adsorption kinetic

Table 10
Comparison of the adsorption capacity between mono and quaternary systems

System	Ions	10 mg L^{-1}	20 mg L^{-1}	30 mg L^{-1}	50 mg L^{-1}	100 mg L^{-1}	200 mg L^{-1}
Mono system	Pb(II)	10	20	30	50	90.58	99.16
	Cd(II)	7.22	12.50	16.12	17.65	21.61	41.74
	Ni(II)	6.17	7.66	8.73	10.76	15.02	32.80
	Cu(II)	9.01	12.61	14.25	15.57	18.00	36.71
Quaternary system	Pb(II)	6.26	8.82	13.03	17.11	23.22	48.23
	Cd(II)	0.92	1.16	1.66	2.83	4.60	8.20
	Ni(II)	0.12	0.31	0.54	1.02	1.35	1.60
	Cu(II)	4.00	4.62	5.18	6.10	8.00	14.91

Note: The relative standard deviation (RSD) is less than 1.0%.

processes of Pb(II), Cd(II), Ni(II), and Cu(II) onto bone char.

- Under the competitive adsorption of multiple heavy metal ions, the q_e of bone char to Pb(II) was considerably higher than that for Cd(II), Ni(II), and Cu(II). Furthermore, Cd(II) and Ni(II) showed a minor impact on Pb(II) adsorption, while Cu(II) exhibited a significant impact.

Acknowledgments

This study was supported by the Natural Science Basic Research Program of Shaanxi Province (2021JM-535) and Special Fund for Scientific Research by Xijing University (XJ18T01).

Symbols

q_e	—	Adsorption capacity at equilibrium, mg g^{-1}
R	—	Removal rate, %
r	—	Solid-to-liquid ratio, g L^{-1}
C_0	—	Initial concentrations of heavy metal ions, mg L^{-1}
C_e	—	Equilibrium concentrations of heavy metal ions, mg L^{-1}
V	—	Volume of the solution, L
m	—	Mass of the adsorbent, g
Q	—	Single-layer maximum adsorption capacity, mg g^{-1}
b	—	Langmuir model constant, L mg^{-1}
R_L	—	Separation factor, dimensionless
K_F	—	Model constant related to the adsorption capacity, mg g^{-1}
n	—	Model constant related to adsorption strength, dimensionless
k_2	—	Adsorption rate constant, g mg^{-1} min^{-1}
q_t	—	Adsorption capacities at time t, mg g^{-1}
h	—	Initial adsorption rate, g mg^{-1} min^{-1}
K_D	—	Distribution coefficient at the solid–liquid interface, mL g^{-1}
T	—	Thermodynamic temperature, K
ΔH	—	Enthalpy change, kJ mol^{-1}
ΔS	—	Entropy change, J mol^{-1} K^{-1}
ΔG	—	Gibbs free energy, kJ mol^{-1}

References

[1] N. Adimalla, J. Chen, H. Qian, Spatial characteristics of heavy metal contamination and potential human health risk assessment of urban soils: a case study from an urban region of South India, Ecotoxicol. Environ. Saf., 194 (2020) 110406, doi: 10.1016/j.ecoenv.2020.110406.
[2] X.J. Long, X. Wang, X.J. Guo, M.C. He, A review of removal technology for antimony in aqueous solution, J. Environ. Sci., 90 (2020) 189–204.
[3] B. Jabłońska, Optimization of Ni(II), Pb(II), and Zn(II) ion adsorption conditions on Pliocene clays from post-mining waste, Miner., 11 (2021) 568, doi: 10.3390/min11060568.
[4] H. Yankovych, V. Novoseltseva, O. Kovalenko, D.M. Behunova, M. Kanuchova, M. Vaclavikova, I. Melnyk, New perception of Zn(II) and Mn(II) removal mechanism on sustainable sunflower biochar from alkaline batteries contaminated water, J. Environ. Manage., 292 (2021) 112757, doi: 10.1016/j.jenvman.2021.112757.
[5] X.H. Wang, Z.F. Zhang, R.Z. Sun, H.Q. Xie, L.G. Yao, High-efficiency removal of low-concentration Hg(II) from aqueous solution by bentonite nanocomposite: batch and fixed-bed column adsorption study, Sep. Sci. Technol., 56 (2021) 2204–2216.
[6] S. Ramola, N. Rawat, A.K. Shankhwar, R.K. Srivastava, Fixed bed adsorption of Pb and Cu by iron modified bamboo, bagasse and tyre biochar, Sustainable Chem. Pharm., 22 (2021) 100486, doi: 10.1016/j.scp.2021.100486.
[7] D.F. Wang, C. Yi, M. Xu, J.S. Park, D. Kim, C.H. Shin, M.H. Ryu, Y.F. Zhao, Adsorption of As(III) and As(V) by using the Fenton reaction modified kapok fiber, J. Environ. Chem. Eng., 9 (2021) 105918, doi: 10.1016/j.jece.2021.105918.
[8] A. Herath, C.A. Layne, F. Perez, E.B. Hassan, C.U. Pittman, T.E. Mlsna, KOH-activated high surface area Douglas Fir biochar for adsorbing aqueous Cr(VI), Pb(II) and Cd(II), Chemosphere, 269 (2021) 128409, doi: 10.1016/j.chemosphere.2020.128409.
[9] G. Sharma, Mu. Naushad, Adsorptive removal of noxious cadmium ions from aqueous medium using activated carbon/zirconium oxide composite: isotherm and kinetic modelling, J. Mol. Liq., 310 (2020) 113025, doi: 10.1016/j.molliq.2020.113025.
[10] Ihsanullah, F.A. Al-Khaldi, B. Abusharkh, M. Khaled, M.A. Atieh, M.S. Nasser, T. Laoui, T.A. Saleh, S. Agarwal, I. Tyagi, V.K. Gupta, Adsorptive removal of cadmium(II) ions from liquid phase using acid modified carbon-based adsorbents, J. Mol. Liq., 204 (2015) 255–263.
[11] C.K. Rojas-Mayorga, D.I. Mendoza-Castillo, A. Bonilla-Petriciolet, J. Silvestre-Albero, Tailoring the adsorption behavior of bone char for heavy metal removal from aqueous solution, Adsorpt. Sci. Technol., 34 (2016) 368–387.
[12] S.A. Begum, A.H.M.G. Hyder, N. Vahdat, Adsorption isotherm and kinetic studies of As(V) removal from aqueous solution using cattle bone char, J. Water Supply Res. Technol. AQUA, 65 (2016) 244–252.
[13] J.V. Flores-Cano, R. Leyva-Ramos, F. Carrasco-Marin, A. Aragon-Pina, J.J. Salazar-Rabago, S. Leyva-Ramos,

Adsorption mechanism of chromium(III) from water solution on bone char: effect of operating conditions, Adsorption, 22 (2016) 297–308.
[14] M.E. Maria, M.B. Mansur, Mathematical modeling of batch adsorption of manganese onto bone char, Braz. J. Chem. Eng., 33 (2016) 373–382.
[15] M.E. Maria, M.B. Mansur, Mathematical modeling of manganese adsorption onto bone char in a continuous fixed bed column incorporating backmixing and shriking core approaches, Braz. J. Chem. Eng., 34 (2017) 901–909.
[16] R.D.C. Soltani, M. Safari, A. Maleki, R. Rezaee, B. Shahmoradi, S. Shahmohammadi, E. Ghahramani, Decontamination of arsenic(V)-contained liquid phase utilizing Fe_3O_4/bone char nanocomposite encapsulated in chitosan biopolymer, Environ. Sci. Pollut. Res., 24 (2017) 15157–15166.
[17] L.E. Hernandez-Hernandez, A. Bonilla-Petriciolet, D.I. Mendoza-Castillo, H.E. Reynel-Avila, Antagonistic binary adsorption of heavy metals using stratified bone char columns, J. Mol. Liq., 241 (2017) 334–346.
[18] J.I. Martins, J.J.M. Orfao, O.S.G.P. Soares, Sorption of copper, nickel and cadmium on bone char, Prot. Met. Phys. Chem. Surf., 53 (2017) 618–627.
[19] N. Ranjbar, S. Hashemi, B. Ramavandi, M. Ravanipour, Chromium(VI) removal by bone char-ZnO composite: parameters optimization by response surface methodology and modeling, Environ. Prog. Sustainable Energy, 37 (2018) 1684–1695.
[20] L. Sellaoui, D.I. Mendoza-Castillo, H.E. Reynel-Avila, A. Bonilla-Petriciolet, A.B. Lamine, A. Erto, A new statistical physics model for the ternary adsorption of Cu^{2+}, Cd^{2+} and Zn^{2+} ions on bone char: experimental investigation and simulations, Chem. Eng. J., 343 (2018) 544–553.
[21] F.A. Gordillo-Ruiz, F.J. Sanchez-Ruiz, D.I. Mendoza-Castillo, H.E. Reynel-Avila, A. Bonilla-Petriciolet, Dynamic fuzzy neural network for simulating the fixed-bed adsorption of cadmium, nickel, and zinc on bone char, Int. J. Environ. Sci. Technol., 15 (2018) 915–926.
[22] J.H. Park, J.J. Wang, S.H. Kim, S.W. Kang, J.S. Cho, R.D. Delaune, Y.S. Ok, D.C. Seo, Lead sorption characteristics of various chicken bone part-derived chars, Environ. Geochem. Health, 41 (2019) 1675–1685.
[23] M.Y. Wang, Y. Liu, Y.M. Yao, L.J. Han, X. Liu, Comparative evaluation of bone chars derived from bovine parts: physicochemical properties and copper sorption behavior, Sci. Total Environ., 700 (2020) 134470, doi: 10.1016/j.scitotenv.2019.134470.
[24] Y.X. Yang, C. Sun, B.C. Lin, Q.X. Huang, Surface modified and activated waste bone char for rapid and efficient VOCs adsorption, Chemosphere, 256 (2020) 127054, doi: 10.1016/j.chemosphere.2020.127054.
[25] N.A. Medellin-Castillo, S.A. Cruz-Briano, R. Leyva-Ramos, J.C. Moreno-Pirajan, A. Torres-Dosal, L. Giraldo-Gutierrez, G.J. Labrada-Delgado, R.O. Perez, J.P. Rodriguez-Estupinan, S.Y.R. Lopez, M.S.B. Mendoza, Use of bone char prepared from an invasive species, pleco fish (*Pterygoplichthys* spp.), to remove fluoride and cadmium(II) in water, J. Environ. Manage., 256 (2020) 109956, doi: 10.1016/j.jenvman.2019.109956.
[26] X.L. Sun, H.Y. Huang, D.L. Zhao, J. Lin, P.C. Gao, L.G. Yao, Adsorption of Pb^{2+} onto freeze-dried microalgae and environmental risk assessment, J. Environ. Manage., 265 (2020) 110472, doi: 10.1016/j.jenvman.2020.110472.
[27] D.D. Do, Adsorption Analysis: Equilibria and Kinetics, Imperial College Press, London, 1998.
[28] S.S. Majumdar, S.K. Das, R. Chakravarty, T. Saha, T.S. Bandyopadhyay, A.K. Guha, A study on lead adsorption by *Mucor rouxii* biomass, Desalination, 251 (2010) 96–102.
[29] B.H. Hameed, J.M. Salman, A.L. Ahmad, Adsorption isotherm and kinetic modeling of 2, 4-D pesticide on activated carbon derived from date stones, J. Hazard. Mater., 163 (2009) 121–126.
[30] S.K. Behera, J.H. Kim, X.J. Guo, H.S. Park, Adsorption equilibrium and kinetics of polyvinyl alcohol from aqueous solution on powdered activated carbon, J. Hazard. Mater., 153 (2008) 1207–1214.
[31] A.E. Ofomaja, Kinetic study and sorption mechanism of methylene blue and methyl violet onto mansonia (*Mansonia altissima*) wood sawdust, Chem. Eng. J., 143 (2008) 85–95.
[32] L.Z. Song, C.Y. Dong, Z.J. Zhang, Q.Y. Zheng, Adsorption behavior of Cu(II) ion by the polyacrylic acid-polyvinylidene fluoride blending resin, China Environ. Sci., 28 (2007) 322–326.
[33] A. Esposito, F. Pagnanelli, A. Lodi, C. Solisio, F. Veglio, Biosorption of heavy metals by *Sphaerotilus natans*: an equilibrium study at different pH and biomass concentrations, Hydrometallurgy, 60 (2001) 129–141.
[34] R. Balasubramanian, S.V. Perumal, K. Vijayaraghavan, Equilibrium isotherm studies for the multicomponent adsorption of lead, zinc, and cadmium onto Indonesian peat, Ind. Eng. Chem. Res., 48 (2009) 2093–2099.
[35] S.H. Abdel-Halim, A.M.A. Shehata, M.F. EI-Shahat, Removal of lead ions from industrial waste water by different types of natural materials, Water Res., 37 (2003) 1678–1683.
[36] S. Meski, S. Ziani, H. Khireddine, Removal of lead ions by hydroxyapatite prepared from the egg shell, J. Chem. Eng. Data, 55(2010) 3923–3928.
[37] F. Boudrahem, F. Aissani-Benissad, H. Aït-Amar, Batch sorption dynamics and equilibrium for the removal of lead ions from aqueous phase using activated carbon developed from coffee residue activated with zinc chloride, J. Environ. Manage., 90 (2009) 3031–3039.
[38] E. Deydier, R. Guilet, P. Sharrock, Beneficial use of meat and bone meal combustion residue: "an efficient low cost material to remove lead from aqueous effluent", J. Hazard. Mater., 101 (2003) 55–64.
[39] P. Waranusantigul, P. Pokethitiyook, M. Kruatrachue, E.S. Upatham, Kinetics of basic dye (methylene blue) biosorption by giant duckweed (*Spirodela polyrrhiza*), Environ. Pollut., 125 (2003) 385–392.
[40] A.E. Ofomaja, Intraparticle diffusion process for lead(II) biosorption onto mansonia wood sawdust, Bioresour. Technol., 101 (2010) 5868–5876.
[41] S.N. Oba, J.O. Ighalo, C.O. Aniagor, C.A. Igwegbe, Removal of ibuprofen from aqueous media by adsorption: a comprehensive review, Sci. Total Environ., 780 (2021) 146608, doi: 10.1016/j.scitotenv.2021.146608.
[42] C.O. Aniagor, C.A. Igwegbe, J.O. Ighalo, S.N. Oba, Adsorption of doxycycline from aqueous media: a review, J. Mol. Liq., 334 (2021) 116124, doi: 10.1016/j.molliq.2021.116124.
[43] H.Y. Chen, X.J. Yang, Y.L. Liu, X.M. Lin, J.J. Wang, Z. Zhang, N. Li, Y.T. Li, Y.L. Zhang, KOH modification effectively enhances the Cd and Pb adsorption performance of N-enriched biochar derived from waste chicken feathers, Waste Manage., 130 (2021) 82–92.
[44] C. Xiong, C. Xue, L.Y. Huang, P. Hu, P. Fan, S.X. Wang, X.T. Zhou, Z.J. Yang, Y.Q. Wang, H.B. Ji, Enhanced selective removal of Pb(II) by modification low-cost bio-sorbent: experiment and theoretical calculations, J. Cleaner Prod., 316 (2021) 128372, doi: 10.1016/j.jclepro.2021.128372.
[45] R. Jayasree, P.S. Kumar, A. Saravanan, R.V. Hemavathy, P.R. Yaashikaa, P. Arthi, J. Shreshta, S. Jeevanantham, S. Karishma, M.V. Arasu, N.A. Al-Dhabi, K.C. Choi, Sequestration of toxic Pb(II) ions using ultrasonic modified agro waste: adsorption mechanism and modelling study, Chemosphere, 285 (2021) 131502, doi: 10.1016/j.chemosphere.2021.131502.
[46] D.M. Wang, W.Y. Luo, J.Y. Zhu, T.F. Wang, Z.J. Gong, M.K. Fan, Potential of removing Pb, Cd, and Cu from aqueous solutions using a novel modified ginkgo leaves biochar by simply one-step pyrolysis, Biomass Convers. Biorefin., (2021), doi: 10.1007/s13399-021-01732-2.
[47] O.A.A. Eletta, F.O. Ayandele, J.O. Lghalo, Adsorption of Pb(II) and Fe(II) by mesoporous composite activated carbon from *Tithonia diversifolia* stalk and *Theobroma cacao* pod, Biomass Convers. Biorefin., (2021), doi: 10.1007/s13399-021-01699-0.
[48] F.D. Meng, Y.W. Zhang, Y.B. Cai, G.D. Yuan, F.X. Han, Kinetic and thermodynamic features of Pb(II) removal from aqueous solution by leonardite-derived humic acid, Water Air Soil Pollut., 232 (2021) 255, doi: 10.1007/s11270-021-05223-y.

[49] D.Z. Shi, H.H. Tong, M.Y. Lv, D. Luo, P. Wang, X.Y. Xu, Z.Y. Han, Optimization of hydrothermal synthesis of hydroxyapatite from chicken eggshell waste for effective adsorption of aqueous Pb(II), Environ. Sci. Pollut. Res., (2021), doi: 10.1007/s11356-021-14772-y.
[50] Z.Z. Wang, J. Xu, D. Yellezuome, R.H. Liu, Effects of cotton straw-derived biochar under different pyrolysis conditions on Pb(II) adsorption properties in aqueous solutions, J. Anal. Appl. Pyrolysis, 157 (2021) 105214, doi: 10.1016/j.jaap.2021.105214.
[51] R. Panek, M. Medykowska, K. Szewczuk-Karpisz, M. Wisniewska, Comparison of physicochemical properties of fly ash precursor, Na-P1(C) zeolite–carbon composite and Na-P1 zeolite—adsorption affinity to divalent Pb and Zn cations, Materials, 14 (2021) 3018, doi: 10.3390/ma14113018.
[52] R. Panek, M. Medykowska, M. Wisniewska, K. Szewczuk-Karpisz, K. Jedruchniewicz, M. Franus, Simultaneous removal of Pb^{2+} and Zn^{2+} heavy metals using fly ash Na-X zeolite and its carbon Na-X(C) composite, Materials, 14 (2021) 2832, doi: 10.3390/ma14112832.
[53] L.S. Tan, Z.H. Ma, K.Q. Yang, Q.L. Cui, K. Wang, T.T. Wang, G.L. Wu, J.Y. Zheng, Effect of three artificial aging techniques on physicochemical properties and Pb adsorption capacities of different biochars, Sci. Total Environ., 699 (2020) 134223, doi: 10.1016/j.scitotenv.2019.134223.
[54] G. Li, J.L. Zhang, J. Liu, C.W. Sun, Z. Yan, Adsorption characteristics of white pottery clay towards Pb(II), Cu(II), and Cd(II), Arabian J. Geosci., 13 (2020) 130–139.
[55] G. Li, J.L. Zhang, J. Liu, S.F. Chen, H.H. Li, Investigation of the adsorption characteristics of Cr(VI) onto fly ash, pine nut shells, and modified bentonite, Desal. Water Treat., 195 (2020) 389–402.
[56] R.C. Xu, Y. Pang, Adsorption characteristics of rice husk biochar on low-concentration Pb(II) from water, Ind. Water Treat., 40 (2020) 35–38.
[57] J.W. Bi, R. Shan, J. Han, H.R. Yuan, Y.Y. Shi, X.Q. Zhang, Preparation of modified watermelon biochar and its adsorption properties for Pb(II), Environ. Sci., 41 (2020) 1770–1778.
[58] Z. L Chen, J.Q. Zhang, L. Huang, Z.H. Yuan, Z.J. Li, M.C. Liu, Removal of Cd and Pb with biochar made from dairy manure at low temperature, J. Integr. Agric., 18 (2019) 201–210.
[59] M. Naushad, Z.A. Alothman, M.R. Awual, M.M. Alam, G.E. Eldesoky, Adsorption kinetics, isotherms, and thermodynamic studies for the adsorption of Pb^{2+} and Hg^{2+} metal ions from aqueous medium using Ti(IV) iodovanadate cation exchanger, Ionics, 21 (2015) 2237–2245.
[60] Y.N. Chen, L.Y. Chai, Y.D. Shu, Study of arsenic(V) adsorption on bone char from aqueous solution, J. Hazard. Mater., 160 (2008) 168–172.
[61] A. Corami, S. Mignardi, V. Ferrini, Cadmium removal from single- and multi-metal (Cd+Pb+Zn+Cu) solutions by sorption on hydroxyapatite, J. Colloid Interface Sci., 317 (2008) 402–408.
[62] A.B. Nasr, K. Walha, C. Charcosset, R.B. Amar, Removal of fluoride ions using cuttlefish bones, J. Fluorine Chem., 132 (2011) 57–62.
[63] E. Valsami-Jones, K.V. Ragnarsdottir, A. Putnis, D. Bosbach, A.J. Kemp, G. Cressey, The dissolution of apatite in the presence of aqueous metal cations at pH 2–7, Chem. Geol., 151 (1998) 215–233.
[64] K.K.H. Choy, G. Mckay, Sorption of metal ions from aqueous solution using bone char, Environ. Int., 31 (2005) 845–854.
[65] E.R. Nightingale, Phenomenological theory of ion solvation effective radii of hydrated ions, J. Phys. Chem., 63 (1959) 1381–1387.
[66] M.G. Goff, F.M. Lambers, T.M. Nguyen, J. Sung, C.M. Rimnac, C.J. Hernandez, Fatigue-induced microdamage in cancellous bone occurs distant from resorption cavities and trabecular surfaces, Bone, 79 (2015) 8–14.
[67] H.F. Wang, P.C. Luo, Preparation, kinetics, and adsorption mechanism study of microcrystalline cellulose-modified bone char as an efficient Pb(II) adsorbent, Water Air Soil Pollut., 231 (2020) 328, doi: 10.1007/s11270-020-04687-8.
[68] M.B. de Estrella, S.T. de Flores, N.A. Bonini, E. Gonzo, N.P. Pérez, A.N. Arias, Rapid synthesis of nanometric cellulose hydroxyapatite, Procedia Mater. Sci., 8 (2015) 608–616.